Optimal optomechanical cavity setups with highly reflecting membranes

Georg Enzian,[1] Eugene S. Polzik,[1] and Alexander K. Tagantsev[2,*]
[1]*Niels Bohr Institute, Quantum Optics Laboratory, Blegdamsvej 17, DK-2100 Copenhagen, Denmark*
[2]*Swiss Federal Institute of Technology, School of Engineering, Institute of Materials Science, CH-1015 Lausanne, Switzerland*

(Received 30 November 2023; revised 15 March 2024; accepted 22 April 2024; published 10 May 2024; corrected 11 September 2024)

Highly reflecting mechanically compliant membranes based on photonic-crystal patterns have recently gained increasing attention within cavity optomechanics due to their prospects of reaching high coupling rates in membrane-in-the-middle experiments. Here, we present an analysis and comparison of four different setups in which highly reflecting membranes can be employed for cavity optomechanics and discuss optimal choices with respect to the figures of merit: cooperativity and efficiency-weighted cooperativity. The analysis encompasses three different types of membrane-in-the-middle setups (membrane at the edge, membrane in the actual middle, and membrane at the back), as well as the simple Fabry-Pérot cavity. Interestingly, we identify and propose the membrane-at-the-back setup as an optimal choice in the limit of negligible membrane parasitic loss, which can reach enormous enhancements of optomechanical cooperativity and, if implemented with a low-loss membrane, would pave the way to nonlinear optomechanics in the quantum regime.

DOI: 10.1103/PhysRevA.109.053514

I. INTRODUCTION

An optical cavity with a mechanically compliant membrane placed inside it is a widely used optomechanical setup. Its typical realization is the so-called membrane-in-the-middle (MIM) cavity, which consists of a Fabry-Pérot optical cavity in which the membrane is placed close to the middle [1–9]. In terms of Fig. 1, for such a configuration, the distance x is set close to $l/2$. Recently, it was identified [10] that, if the membrane is highly reflecting and properly positioned close to the input mirror, the optomechanical coupling constant of the system can be appreciably increased compared to the MIM configuration. This configuration was called "membrane at the edge"(MATE). Reference [10] showed that, for MATE, a regime exists where the optomechanical coupling constant increases inversely proportionally to the membrane transmission. Since, currently, mechanical membranes with an extremely low transmission are available [11–13], efficient use of highly reflecting membranes in optomechanical cavity setups is an issue of appreciable interest.

In this paper, we theoretically address the configuration in which a highly reflecting membrane is positioned close to the backstop mirror, which we call "membrane at the back" (MAK). We compare the optimized optomechanical performance of the three aforementioned configurations using the optomechanical cooperativity and the efficiency-weighted cooperativity as figures of merit. Only the dispersive optomechanical coupling, which typically dominates the systems, is taken into account.

In contrast to previous theoretical considerations of an optical cavity with a membrane inside [1,2,10], we take into consideration the parasitic scattering from the membrane while neglecting the parasitic scattering from the coupling mirror, which we assume is much weaker than that from the membrane. We demonstrate that, in the case of a highly reflecting membrane, even a small amount of parasitic scattering from the membrane may have an essential impact on the cooperativity of the system.

In the case of a highly reflecting membrane, the spectrum of the cavity is close to the superposition of those of the two subcavities, being strongly affected near the crossing points of these spectra by the effect of avoided crossing. At the avoided-crossing points, the dispersive optomechanical coupling vanishes. Evidently, halfway between these points, the suppressing effect of the avoided crossing on the dispersive coupling is minimal. As we are interested in the best performance of the system, this paper will focus on these "halfway" points.

We will show that, for highly reflecting membranes, in terms of the cooperativity, MAK is always appreciably more advantageous than MIM, while, depending on the parameters of the system, MAK either is appreciably more advantageous than MATE or the performance of MATE is very close to that of MAK.

We will also compare the MAK scheme with a simple Fabry-Pérot (FP) cavity, with the highly reflecting membrane playing the role of the coupling mirror. We will show that, depending on the parameters of the systems, MAK can be more or less advantageous than a FP cavity whose length is equal to the membrane-mirror separation in MAK.

II. SYSTEM MODEL

To be specific, we set the following scattering matrices:

$$\begin{pmatrix} it & -r \\ -r & it \end{pmatrix} \tag{1}$$

*alexander.tagantsev@epfl.ch

for the input mirror,

$$\begin{pmatrix} 0 & -1 \\ -1 & 0 \end{pmatrix} \tag{2}$$

for the backstop mirror, and

$$\begin{pmatrix} t_m e^{i\varphi_t} & r_m e^{i\varphi_r} \\ r_m e^{i\varphi_r} & t_m e^{i\varphi_t} \end{pmatrix} \tag{3}$$

for the membrane. In matrices (1), (2), and (3), the amplitude transmission coefficients are on the diagonals. Here, all parameters, including phases φ_t and φ_r, are set as real and positive, while

$$t^2 + r^2 = 1, \quad e^{2i(\varphi_r - \varphi_t)} = -1. \tag{4}$$

The finesse of the cavity is assumed to be high:

$$t \ll 1. \tag{5}$$

Although the treatment of cavities with a membrane inside is typically done by neglecting parasitic scatting of the membrane, i.e., assuming $t_m^2 + r_m^2 = 1$, we incorporate it in our consideration since, as will be seen below, such scattering may strongly affect the behavior of the system addressed. Specifically, we set

$$t_m^2 + r_m^2 = 1 - t_s^2, \tag{6}$$

where t_s^2 is the power-scattering coefficient associated with the aforementioned scattering.

Throughout the paper we restrict ourselves to the case of a highly reflecting membrane, i.e.,

$$t_m^2 \ll 1. \tag{7}$$

As seen from Eqs. (2) and (4), we neglect the parasitic scattering against the coupling mirror and the finite transmission of the backstop mirror. This is justified under the reasonable assumptions that the above scattering is much weaker than the coupling mirror transmission and the power transmission of the backstop is much smaller than t_s^2.

III. BASIC FEATURES OF AN OPTICAL CAVITY WITH A HIGHLY REFLECTING MEMBRANE INSIDE

In this section, we address some basic features of an optical cavity with a highly reflecting membrane inside. We do this while neglecting the dissipation effects in the system.

Let us start from the case of a perfectly reflecting membrane ($t_m = 0$). In this case, the resonance spectrum of the system for any position of the membrane is just the sum of the spectra of its right and left subcavities, as shown in Fig. 2. The resonance frequencies of the modes of the left part ω_L decrease with increasing x, while those of the modes of the right part ω_R increase. Hereafter, we denote these modes as ω_L modes and ω_R modes, respectively. For small, but finite, t_m, the spectrum shown in Fig. 2 provides a good approximation for the spectrum except in the vicinity of the crossing points where an avoided crossing takes place, resulting in the formation of a small gap. Away from avoided crossing points, we can still retain unambiguous nomenclature, ω_L modes and ω_R modes, to classify the modes. The modification of the spectrum caused by the variation of t_m is illustrated in Fig. 3.

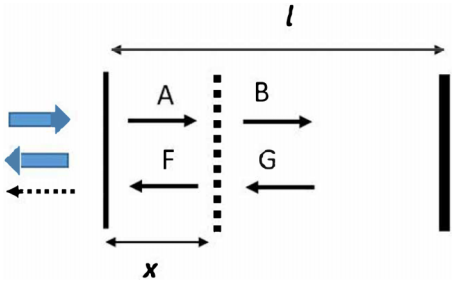

FIG. 1. A one-sided cavity with a mechanical semitransparent membrane set inside it. The dashed line represents the membrane, the thin solid line represents the semitransparent input mirror, the thick solid line represents the perfectly reflecting back-stop mirror, the thick arrows represent the pump light, and the dashed arrow represents the detected light. The waves inside the cavity are shown with arrows which are marked with their complex amplitudes.

Here, the effect of avoided crossings at the crossing points is seen. Three crossing points are marked with circles. An important feature of the avoided crossing is that this effect becomes stronger when the membrane approaches the mirrors of the cavity. The strength of this effect can be quantified by the frequency gap $\delta\omega$, which appears at the crossing point. Using the well-known equation

$$\cos(kl + \varphi_r) = -r_m \cos(2kx - kl) \tag{8}$$

for the resonant wave vector k of an optical cavity with a semitransparent mirror inside (see, e.g., [10]), which neglects the energy decay in the cavity, in the limit $t_m \ll 1$, one finds (see Appendix A)

$$\delta\omega \propto \frac{ct_m}{\sqrt{x_0(l - x_0)}}, \tag{9}$$

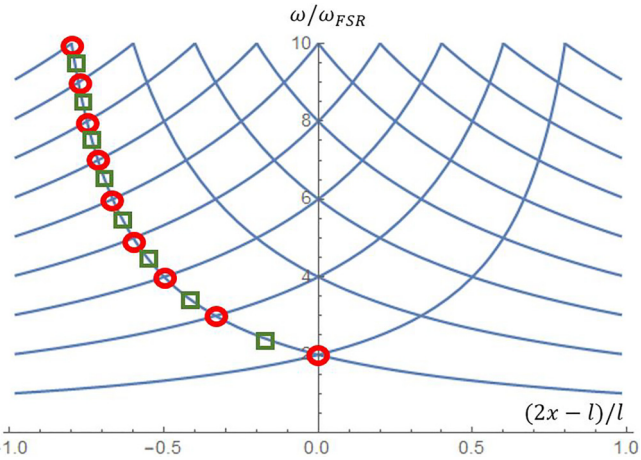

FIG. 2. The spectrum of an optical cavity with a perfectly reflecting membrane inside ($r_m = 1$) as a function of the membrane position. The phase shift at reflection from the membrane is set as $\varphi_r = \pi$. $\omega_{FSR} = \pi c/l$ is the free spectral range of the empty cavity, where l is the cavity length and c is the speed of light. For a selected ω_L mode, the places where it crosses a number of ω_R modes are marked with the circles. The r points, where the selected ω_L mode is on resonance while the ω_R modes are on antiresonance, are marked with the squares.

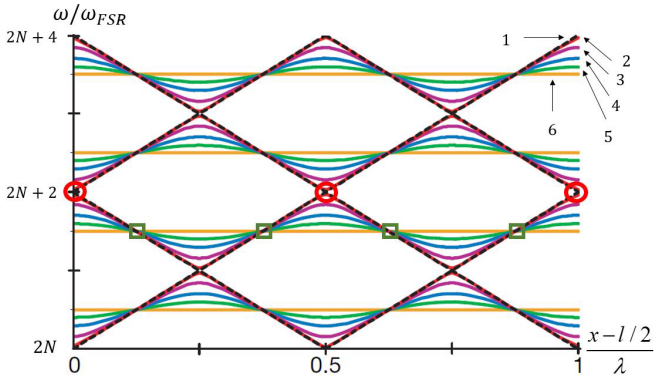

FIG. 3. Part of the spectrum of an optical cavity with a semitransparent membrane inside for high-order cavity resonances ($N \gg 1$ is an integer) plotted for different values of the amplitude transmission coefficients t_m: (1) 0, (2) 0.1, (3) 0.48, (4) 0.8, (5) 0.95, and (6) 1. $\omega_{\rm FSR}$ is the free spectral range of the empty cavity. The phase shift at reflection from the membrane is set as $\varphi_r = \pi$. Three crossing points are marked with circles. Four r points are marked with squares. This figure is based on the results from Ref. [4].

where x_0 is the distance from a crossing point to the left mirror of the cavity and c is the speed of light. Equation (9) justifies the above statement.

The solution to Eq. (8) also yields [see Eqs. (A2)]

$$\omega_0 = \omega_{\rm FSR}\left(N - \frac{\varphi_r}{\pi}\right) \tag{10}$$

for the frequency of the crossing points ω_0, where $\omega_{\rm FSR} = \pi c/l$ is the free spectral range of the empty cavity, l is the cavity length, and N is an integer.

Another remarkable feature of the system, which is seen in Fig. 3, is that the positions of the points where the dispersion curves of the decoupled modes (the straight lines) cross the dispersion curves of the system (at finite membrane transmission t_m) are not sensitive to the value of t_m (see Appendix B). In Fig. 3, four such points are marked with squares. With the variation of t_m, the $\omega(x)$ curves "locally rotate" about such points. We call these points "r points."

The solution to Eq. (8) yields [see Eqs. (B1), (B2), and (B3)]

$$\omega_r = \omega_{\rm FSR}\left(\frac{1}{2} + N - \frac{\varphi_r}{\pi}\right) \tag{11}$$

for the frequency of the r points.

Figure 2 illustrates the relative position of the points of avoided crossing and r points on an $\omega_{\rm L}$ branch of the spectrum. It is seen that, in frequency, these are separated by $\omega_{\rm FSR}/2$, which follows from Eqs. (10) and (11). In other words, each r point lies in the middle of two neighboring points of avoided crossing. The avoided crossing obviously results in a reduction in the slopes of the $\omega(x)$ curves and, as a result, in a reduction of the optomechanical coupling. It is clear that the middle position of the r points between neighboring points of avoided crossing makes the r points favorable in terms of such coupling.

For this reason, in the discussion below, we will focus on these points. This discussion will be based on the following properties of the system at the r points. The derivation of these properties is given in Appendix B. Here, we just list them.

At the r points one of the subcavities is on resonance, while the other is on antiresonance. Mathematically, in terms of the resonance wave vectors k, this means that, for $\omega_{\rm L}$ modes,

$$e^{-2ik_0(l-x)-i\varphi_r} = 1, \quad e^{-2ik_0x-i\varphi_r} = -1, \tag{12}$$

while for $\omega_{\rm L}$ modes,

$$e^{-2ik_0(l-x)-i\varphi_r} = -1, \quad e^{-2ik_0x-i\varphi_r} = 1. \tag{13}$$

For the r points and the case of highly reflecting membranes, the ratio of the field intensity in one part of the cavity to that in the other part is fully controlled by the power (intensity) transmission of the membrane $T_m = t_m^2$. Specifically, for the $\omega_{\rm L}$ mode,

$$\frac{|B|^2}{|A|^2} = \frac{T_m}{4}, \tag{14}$$

where $|A|^2$ and $|B|^2$ are the intensities in the x-long and $l-x$-long parts of the cavity, respectively. For $\omega_{\rm R}$ mode, we have

$$\frac{|B|^2}{|A|^2} = \frac{4}{T_m}. \tag{15}$$

As seen from Fig. 3, once the membrane is close to the middle of the cavity, for small t_m, the slope of the $\omega(x)$ curves at the r points is hardly affected by the coupling between the subcavities. However, as was shown above, the effect of such coupling increases when the membrane approaches one of the cavity mirrors. Thus, for small distances between the membrane and the mirror, the impact of this coupling on the aforementioned slope may become appreciable. Let us introduce the critical membrane-mirror separation, which we denote $x_{\rm int}$, at which this happens. We mean that at $x_{\rm int} \ll x \ll l$ the effect on the intercavity coupling of the spectrum near the r points is negligible, while at $x \ll x_{\rm int} \ll l$, it is very strong. These two regimes can also be viewed in terms of the mode energy. At $x_{\rm int} \ll x \ll l$, the subcavities are virtually decoupled such that the energy of the $\omega_{\rm L}$ mode, such as that originating from the smaller left subcavity, should be mainly stored in this subcavity. On the other hand, for $x \ll x_{\rm int} \ll l$, since now the intercavity coupling is very strong, the main fraction of energy of the $\omega_{\rm L}$ mode should be stored in the larger right subcavity. In view of the above we determine $x_{\rm int}$ from the condition that, at $x = x_{\rm int}$, the energy of the $\omega_{\rm L}$ mode is equally distributed between the two subcavities. This condition readily yields (see Appendix B)

$$x_{\rm int} = l\frac{T_m}{4}, \tag{16}$$

where $T_m = t_m^2$ is the power (intensity) transmission of the membrane.

Evidently, for the $\omega_{\rm R}$ mode, $x_{\rm int}$ also represents the corresponding critical separation between the membrane and the backstop mirror.

IV. DISPERSIVE COUPLING FOR AN OPTICAL CAVITY WITH A HIGHLY REFLECTING MEMBRANE INSIDE

In this section, we consider the dispersive optomechanical coupling at the r points. Since we are interested in the case

TABLE I. The absolute values of the dispersive optomechanical coupling constants normalized to the MIM coupling constant $g_0/(2\omega_c x_{\rm zpf}/l)$ for the $\omega_{\rm L}$ and $\omega_{\rm R}$ modes at the r points for three configurations: $x \ll x_{\rm int}$, $|x - l/2| \ll l$, and $l - x \ll x_{\rm int}$, which are labeled MATE, MIM, and MAK, respectively. T_m is the power-transmission coefficient of the membrane. The values for MATE for the $\omega_{\rm L}$ mode and for MAK for the $\omega_{\rm R}$ mode given in this table are valid to within a factor of 1/2 for the membrane-mirror separation equal to $x_{\rm int}$.

	MATE	MIM	MAK
$\omega_{\rm L}$	$2/T_{\rm m}$	1	1/2
$\omega_{\rm R}$	1/2	1	$2/T_{\rm m}$

of weak dissipation effects, in this section, we evaluate the spectrum of the system while neglecting these effects.

We define the dispersive coupling constant of the system as follows:

$$g_0 = -\frac{d\omega_c}{dx} x_{\rm zpf}, \tag{17}$$

where ω_c is the resonance frequency of the system and $x_{\rm zpf}$ is the amplitude of zero-point fluctuations. Let us first address g_0 of the $\omega_{\rm L}$ mode. According to Sec. III, at $l - x_{\rm int} \gg x \gg x_{\rm int}$, the dispersive coupling for the decoupled $\omega_{\rm L}$ mode, i.e., at $t_m = 0$, provides a good approximation for that at finite t_m, implying

$$g_0 = \frac{\omega_c}{x} x_{\rm zpf}. \tag{18}$$

Here, the $1/x$ increase in g_0 at $x \to 0$ results from the confinement of the mode energy in a decreasing volume. At x approaching $x_{\rm int}$, this trend saturates such that one can reasonably suppose that at $x \ll x_{\rm int}$

$$g_0 = \frac{\omega_c}{x_{\rm int}} x_{\rm zpf}, \quad x_{\rm int} = l\frac{T_m}{4}. \tag{19}$$

The result given by (19) is consistent with the enhanced value of g_0, which was identified for the system in Ref. [10].

Such a heuristic result is readily supported by direct calculations. We rewrite the resonance equation (8) in the following equivalent form (see Appendix D):

$$(r_m + e^{-2ik(l-x)-i\varphi_r})(r_m + e^{-2ikx-i\varphi_r}) + 1 - r_m^2 = 0, \tag{20}$$

and we calculate $\frac{dk}{dx}$ at k satisfying Eq. (12). Next, using (17) and taking into account that $T_m \ll 1$, we find (see Appendix D)

$$g_0 = \frac{\omega_c}{x + x_{\rm int}} x_{\rm zpf}, \tag{21}$$

justifying (19).

The above heuristic argument holds for the $\omega_{\rm R}$ mode, while the direct calculation involving (20) and (13) yields (see Appendix D)

$$g_0 = -\frac{\omega_c}{l - x + x_{\rm int}} x_{\rm zpf}. \tag{22}$$

Next, based on Eqs. (21) and (22), in Table I, we summarize the values of $|g_0|$ for three regimes, where $x \ll x_{\rm int}$, $|x - l/2| \ll l$, and $l - x \ll x_{\rm int}$, which we label MATE, MIM, and MAK, for the membrane-at-the-edge, membrane-in-the-middle, and membrane-at-the-back systems, respectively. In Table I, the values of $|g_0|$ given for MATE for the $\omega_{\rm L}$ mode and for MAK for the $\omega_{\rm R}$ mode are the same, being the upper limit for $|g_0|$ in this system. The values for MATE for the $\omega_{\rm L}$ mode and for MAK for the $\omega_{\rm R}$ mode given in Table I are valid to within a factor of 1/2 for the membrane-mirror separation equal to $x_{\rm int}$. Table I suggests that, with respect to dispersive coupling, MATE and MAK yield a performance which, for highly reflecting membranes, is substantially superior to that of MIM.

V. CAVITY LINEWIDTH AND COOPERATIVITY OF AN OPTICAL CAVITY WITH A HIGHLY REFLECTING MEMBRANE INSIDE

The dispersive coupling constant g_0 evaluated above does not represent, in general, a reliable optomechanical figure of merit. An appropriate figure of merit for mechanical sensing [14] and optomechanical squeezing [15] is the so-called single-photon cooperativity, which reads

$$C = \frac{4g_0^2}{\kappa\gamma_m}, \tag{23}$$

where κ is the optical decay rate and γ_m is the mechanical decay rate. C is a fully appropriate parameter in the case where the linewidth of the system is controlled only by the energy leakage though the coupling mirror. However, once the parasitic scattering against the membrane is involved, after stating that the linewidth can be decomposed into contributions from external coupling and parasitic loss,

$$\kappa = \kappa_{\rm ext} + \kappa_s, \tag{24}$$

we can define the efficiency-weighted cooperativity

$$C_\eta = \eta C = \frac{4g_0^2\kappa_{\rm ext}}{(\kappa_{\rm ext} + \kappa_s)^2\gamma_m}, \tag{25}$$

where we introduced the coupling efficiency η as

$$\eta = \frac{\kappa_{\rm ext}}{\kappa}. \tag{26}$$

We can readily check that, for optical sensing of the mechanical subsystem, it is the efficiency-weighted cooperativity that plays the role of the figure of merit.

A. Simple estimates and qualitative arguments

Prior to a more detailed analysis, we compare the cooperativity performance of MATE, MIM, and MAK in the standard framework [1,10] with the parasitic scattering of the membrane neglected; i.e., we set $t_s = 0$ [see Eq. (6)]. We do this for the r points and for the regime where MATE and MIM yield the maximum g_0, i.e., for the membrane separations from the adjacent mirror, which are much smaller than $x_{\rm int} = l\frac{T_m}{4}$.

The optical decay rates of MATE, MIM, and MAK can readily be found from the field distributions in these systems shown in Fig. 4 and the standard definition (see, e.g., [10]) of the decay rate:

$$\kappa = \frac{\text{dissipated power}}{\text{stored energy}} = \frac{ct^2 W(0)}{2l\bar{W}}, \tag{27}$$

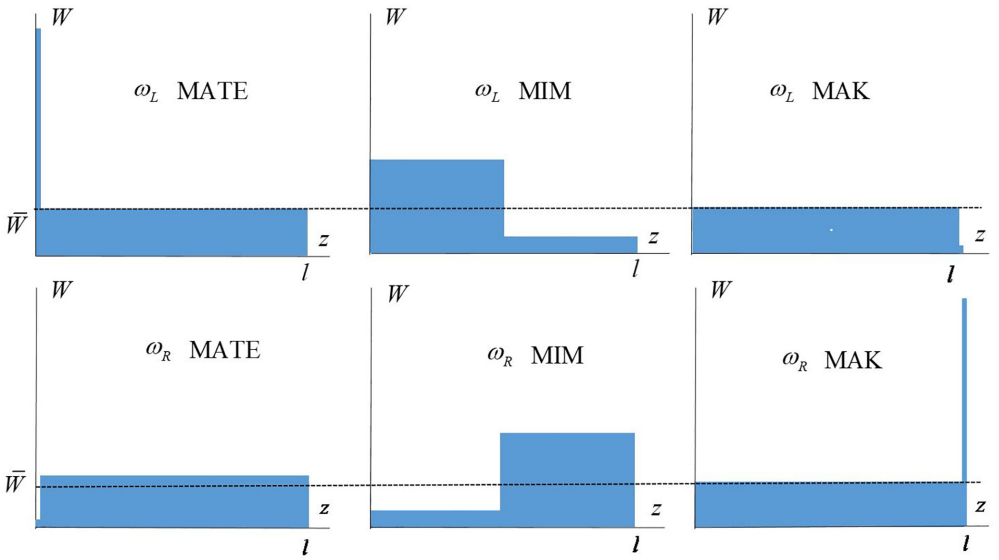

FIG. 4. The distribution of the field intensity in the MATE, MIM, and MAK configurations at r points for the ω_{L} and ω_{R} modes. $\bar{W}$ denotes the field intensity averaged over the cavity. For MATE and MAK, the regime where the membrane separation from the adjacent mirror is much smaller than $x_{\mathrm{int}} = l\frac{T_m}{4}$ is considered. This figure is not to scale.

where $W(0)$ and $\bar{W}$ are the optical field intensity at the input mirror and the optical field intensity averaged over the cavity. Since the case of weak dissipative effects is addressed, Eqs. (14) and (15), which were obtained while neglecting the dissipation, can be used for the evaluation of $W(0)$ and $\bar{W}$. Figure 4 schematically illustrates the relations between the field intensities given by Eqs. (14) and (15). For MIM, using (14) and (15), we can write

$$W(0) \approx 2\bar{W} \quad \text{for } \omega_L,$$
$$W(0) \approx \frac{T_m}{2}\bar{W} \quad \text{for } \omega_R. \tag{28}$$

As for MATE and MAK, taking into account that, in the addressed regime where the membrane separation from the adjacent mirror is much smaller than x_{int}, the energy of the mode is mainly stored in the larger subcavities, we find that for MATE

$$W(0) \approx \frac{4}{T_m}\bar{W} \quad \text{for } \omega_L,$$
$$W(0) \approx \frac{T_m}{4}\bar{W} \quad \text{for } \omega_R, \tag{29}$$

while, in MAK, for both modes

$$W(0) \approx \bar{W}. \tag{30}$$

Next, using the above results, those from Table I, and Eqs. (27) and (23), we arrive at the results for the cavity linewidth and cooperativity C, which are summarized in Tables II and III. From Table III we conclude that for an ideal membrane, i.e., a membrane exhibiting no parasitic scattering, with respect to the cooperativity, despite higher g_0 MATE is not advantageous compared to MIM, while MAK is strongly advantageous (by at least $2/T_m$ times) compared to other systems.

Another conclusion can be drawn from scrutinizing Fig. 4. It is seen that, for the ω_{R} mode in MIM and MAK, which, according to Table III, are the two most advantageous cases, the reflecting membrane is in contact with a field which is much larger than that at the coupling mirror. This suggests that even very small parasitic scattering may be detrimental for the linewidth and cooperativity for these systems. In the next section, we will address this matter in detail.

B. Linewidth and cooperativity in the presence of parasitic scattering

In order to calculate the linewidth of the system, one can generalize Eq. (8), which is written for the real resonance wave vector, to the following resonance equation for the complex wave vector k (see Appendix D):

$$(r_m + e^{-2ik(l-x)-i\varphi_r})(r_m + r^{-1}e^{-2ikx-i\varphi_r}) + 1 - r_m^2 = T_s, \tag{31}$$

where $T_s = t_s^2$ is the power-scattering coefficient associated with the parasitic scattering [see Eq. (6)]. Next, one finds the linewidth κ as follows:

$$\kappa = -2c\mathrm{Im}[k]. \tag{32}$$

TABLE II. The normalized cavity linewidth κ/κ_0, where $\kappa_0 = cT/l$, for the ω_{L} and ω_{R} modes at three configurations: $x \ll x_{\mathrm{int}}$, $|x - l/2| \ll l$, and $l - x \ll x_{\mathrm{int}}$, which are labeled MATE, MIM, and MAK, respectively. T and T_m are the power-transmission coefficients of the coupling mirror and membrane, respectively. The values for MATE for the ω_{L} mode and for MAK for the ω_{R} mode given in this table are valid to within a factor of 1/2 for the membrane-mirror separation equal to x_{int}. The results are valid for the r points of the spectrum.

	MATE	MIM	MAK
ω_{L}	$2/T_m$	1	1/2
ω_{R}	$T_m/8$	$T_m/4$	1/2

TABLE III. The normalized cooperativity C/C_0, $C_0 = 16(\omega_c x_{\rm zpf})^2/(Tcl\gamma_m)$, for the $\omega_{\rm L}$ and $\omega_{\rm R}$ modes at three configurations: $x \ll x_{\rm int}$, $|x - l/2| \ll l$, and $l - x \ll x_{\rm int}$, which are labeled MATE, MIM, and MAK, respectively. T and T_m are the power-transmission coefficients of the coupling mirror and membrane, respectively. The values for MATE for the $\omega_{\rm L}$ mode and for MAK for the $\omega_{\rm R}$ mode given in this table are valid to within a factor of 1/2 for the membrane-mirror separation equal to $x_{\rm int}$. The results are valid for the r points of the spectrum.

	MATE	MIM	MAK
$\omega_{\rm L}$	$2/T_m$	1	1/2
$\omega_{\rm R}$	$2/T_m$	$4/T_m$	$8/T_m^2$

Being interested in the r points of the spectrum in the regime of small damping, we are looking for a solution to (31) written in the form $k = k_0 + \delta k$, where k_0 is the real solution to Eq. (8) at these points. Since the situation of a weak dissipation is addressed, implying $|\delta k| \ll |k_0|$, such that δk can be calculated by linearizing Eq. (31). In this way, using (32) (see Appendix D) for the $\omega_{\rm R}$ mode, one finds

$$\kappa_{\rm ext} = \frac{c}{2}\frac{TT_m/4}{l - x + x_{\rm int}}, \tag{33}$$

$$\kappa_s = \frac{c}{2}\frac{T_s}{l - x + x_{\rm int}}, \tag{34}$$

implying the efficiency

$$\eta = \frac{TT_m/4}{T_s + TT_m/4}. \tag{35}$$

For the $\omega_{\rm L}$ mode, one finds

$$\kappa_{\rm ext} = \frac{c}{2}\frac{T}{x + x_{\rm int}}, \tag{36}$$

$$\kappa_s = \frac{c}{2}\frac{T_s}{x + x_{\rm int}}, \tag{37}$$

implying the efficiency

$$\eta = \frac{T}{T_s + T}. \tag{38}$$

Here, $T = t^2$ is the power-transmission coefficient of the coupling mirror.

We can easily see that the cooperativity calculated while neglecting the parasitic scattering against the membrane should be multiplied by the efficiency to yield the cooperativity calculated while taking it into account. Thus, using Table III and Eqs. (35) and (38), we arrive at the results listed in Table IV.

The results presented in Table IV can be summarized as follows. We discuss the $\omega_{\rm R}$ regime of MAK, the $\omega_{\rm R}$ regime of MIM, and the $\omega_{\rm L}$ regime of MATE. The "standing" of those regimes depends on the position of T_s with respect to $TT_m/4$ and T. At $T_s \ll TT_m/4$, we are back to the dissipation-free regime, and MAK is more advantageous than other regimes by a factor of about $1/T_m$. At $TT_m/4 \ll T_s \ll T$, MAK is more advantageous than MIM by a factor of about $1/T_m$ and is more advantageous than MATE by a factor of about T/T_s. Finally, at $T_s \gg T$, MAK and MATE yield practically the same cooperativity and are more advantageous than MIM by a factor of about $1/T_m$. All in all, it is seen that, once the parasitic scattering against the membrane is taken into account, in terms of the cooperativity, MAK is the best, although, at $T_s \gg T$, the performance of MATE is very close to that of MAK.

TABLE IV. Cooperativity calculated taking into account the parasitic scattering of the membrane. The normalized cooperativity C/C_0, where $C_0 = 16(\omega_c x_{\rm zpf})^2/(Tcl\gamma_m)$, for the $\omega_{\rm L}$ and $\omega_{\rm R}$ modes at three configurations: $x \ll x_{\rm int}$, $|x - l/2| \ll l$, and $l - x \ll x_{\rm int}$, which are labeled MATE, MIM, and MAK, respectively. Here, $T_s = t_s^2$, $T = t^2$, and $T_m = t_m^2$, are the power-scattering coefficients associated with the parasitic scattering and the power-transmission coefficients of the coupling mirror and membrane, respectively. The values for MATE for the $\omega_{\rm L}$ mode and for MAK for the $\omega_{\rm R}$ mode given in this table are valid to within a factor of 1/2 for the membrane-mirror separation equal to $x_{\rm int}$. The results are valid for the r points of the spectrum.

	MATE	MIM	MAK
$\omega_{\rm L}$	$\frac{2T}{T_m(T_s+T)}$	$\frac{T}{T_s+T}$	$\frac{T/2}{T_s+T}$
$\omega_{\rm R}$	$\frac{T/2}{T_s+TT_m/4}$	$\frac{T}{T_s+TT_m/4}$	$\frac{2T}{T_m(T_s+TT_m/4)}$

It is instructive to give general expressions for the cooperativity of the $\omega_{\rm R}$ and $\omega_{\rm L}$ modes. Using Eqs. (21), (22), (23), (24), (33), (34), (36), and (37), we find

$$C = \frac{8}{c\gamma_m}\frac{(\omega_c x_{\rm zpf})^2}{x + x_{\rm int}}\frac{1}{T_s + T} \tag{39}$$

for the $\omega_{\rm L}$ mode and

$$C = \frac{8}{c\gamma_m}\frac{(\omega_c x_{\rm zpf})^2}{l - x + x_{\rm int}}\frac{1}{T_s + TT_m/4} \tag{40}$$

for the $\omega_{\rm R}$ mode. It is clear from these expressions that, moving from the optimal regime for MATE with the $\omega_{\rm L}$ mode and for MAK with the $\omega_{\rm R}$ mode where the mirror-membrane separation δ is much smaller than $x_{\rm int}$ to the regime with $\delta = x_{\rm int}$, the cooperativity decreases by only a factor of 2.

C. Efficiency-weighted cooperativity

Multiplying Eqs. (39) and (40) by the efficiency given by Eqs. (35) and (38), we find

$$C_\eta = \frac{8}{c\gamma_m}\frac{(\omega_c x_{\rm zpf})^2}{x + x_{\rm int}}\frac{T}{(T_s + T)^2} \tag{41}$$

for the efficiency-weighted cooperativity of the $\omega_{\rm L}$ mode and

$$C_\eta = \frac{8}{c\gamma_m}\frac{(\omega_c x_{\rm zpf})^2}{l - x + x_{\rm int}}\frac{TT_m/4}{(T_s + TT_m/4)^2} \tag{42}$$

for the efficiency-weighted cooperativity of the $\omega_{\rm R}$ mode. We see that both expressions can be maximized by changing T, T_m, or T_s to match the internal and external losses.

For the $\omega_{\rm L}$ mode, the maximum is reached at $T = T_s$, yielding

$$C_{\eta,\,\max} = \frac{4}{c\gamma_m}\frac{(\omega_c x_{\rm zpf})^2}{x + x_{\rm int}}\frac{1}{T_s}, \tag{43}$$

while for the ω_R mode, the maximum condition reads

$$TT_m/4 = T_s, \tag{44}$$

such that

$$C_{\eta,\,\max} = \frac{4}{c\gamma_m}\frac{(\omega_c x_{\rm zpf})^2}{l - x + x_{\rm int}}\frac{1}{T_s}. \tag{45}$$

Applying the above expression to MIM, we find

$$C^{\rm MIM}_{\eta,\,\max} = \frac{8}{c\gamma_m}\frac{(\omega_c x_{\rm zpf})^2}{l}\frac{1}{T_s}. \tag{46}$$

As for MAK and MATE, if we denote the separation between the membrane and the nearest mirror as δ, Eqs. (43) and (45) yield the same result,

$$C^{\rm MATE,\,MAK}_{\eta,\,\max} = \frac{4}{c\gamma_m}\frac{(\omega_c x_{\rm zpf})^2}{\delta + x_{\rm int}}\frac{1}{T_s}. \tag{47}$$

Here, the following reservation is needed. For highly reflecting membranes, condition (44) may not be met such that the efficiency-weighted cooperativity of MAK may not be optimized up to the value given by Eq. (47).

Comparing Eq. (46) with (47), since for MAK and MATE, as agreed, $\delta \ll l$, we clearly see that, with respect to the optimized efficiency-weighted cooperativity, MATE and MAK are better than MIM.

VI. MAK AND MATE VERSUS A SHORT FABRY-PÉROT CAVITY

In the discussion above, we addressed the problem of the optimal placement of a highly reflecting membrane in a one-sided cavity. We did that for the points of the spectrum where g_0 is less affected by the effect of the avoided crossing of the resonance modes of the two subcavities, which we called r points. We found that MIM is always less effective than MAK and MATE. A remarkable feature of MAK and MATE at the r points is that the shorter subcavity is on resonance while the longer one is on antiresonance. Actually, MATE can be formally viewed as a short cavity with a synthetic backstop mirror, while MAK can be viewed as one with a synthetic coupling mirror with the reservation that, in the regime of interest, the energy of the modes used is not mainly stored in the shorter subcavity. In this context, it is of interest to compare the performance of MAK and MATE, which have membrane-mirror separation δ, with the performance of a one-sided FP cavity, which have length δ, using the membrane as the coupling mirror.

We readily find the following principle parameters of FP:

$$g_0^{\rm FP} = \frac{\omega_c}{\delta}x_{\rm zpf}, \tag{48}$$

$$\kappa_{\rm ext,}^{\rm FP} = \frac{cT_m}{2\delta}, \quad \kappa_s^{\rm FP} = \frac{cT_s}{2\delta}, \tag{49}$$

$$C^{\rm FP} = \frac{8}{c\gamma_m}\frac{(\omega_c x_{\rm zpf})^2}{\delta}\frac{1}{T_s + T_m}, \tag{50}$$

$$C_\eta^{\rm FP} = \frac{8}{c\gamma_m}\frac{(\omega_c x_{\rm zpf})^2}{\delta}\frac{T_m}{(T_s + T_m)^2}, \tag{51}$$

$$C^{\rm FP}_{\eta,\,\max} = \frac{4}{c\gamma_m}\frac{(\omega_c x_{\rm zpf})^2}{\delta}\frac{1}{T_s}. \tag{52}$$

Comparing g_0, i.e., (21), (22), and (48), we find that FP is advantageous by a factor of $\frac{x_{\rm int}+\delta}{\delta}$. The same factor controls the superiority of FP in the case of the optimized efficiency-weighted cooperativity [see (47) and (52)].

For the cooperativity, we compare FP with MAK, which, with respect to this parameter, is the best configuration with the membrane inside the cavity. Thus, we compare (50) with (40) rewritten as follows:

$$C^{\rm MAK} = \frac{8}{c\gamma_m}\frac{(\omega_c x_{\rm zpf})^2}{\delta + lT_m/4}\frac{1}{T_s + TT_m/4}. \tag{53}$$

First, we address the regime of extremely low parasitic scattering where T_s is smaller than or about $TT_m/4$. In this regime, MAK is strongly advantageous compared to other configurations with a highly reflecting membrane inside the cavity. We can readily check that, for not too long cavities, that is, for

$$l \ll \frac{4\delta}{T_m}, \tag{54}$$

MAK is more advantageous than FP by a factor of $\frac{4(T_m+T_s)}{T_mT}$, which can lead to a few-order-of-magnitude gain.

Such a regime, however, is not realistic for currently available systems with highly reflecting membranes, where $T_s \gg TT_m/4$. At $T_s \gg TT_m/4$, (50) and (53) can be simplified to

$$C^{\rm FP} = \frac{C_s}{1 + \frac{T_m}{T_s}}, \tag{55}$$

$$C^{\rm MAK} = \frac{C_s}{1 + \frac{l}{\delta}\frac{T_m}{4}}, \tag{56}$$

where

$$C_s = \frac{8}{c\gamma_m}\frac{(\omega_c x_{\rm zpf})^2}{\delta T_s} \tag{57}$$

is the cooperativity of FP in the limit where the loss is fully dominated by the parasitic scattering. Comparing (55) with (56), we find that, in cavities shorter than $l_0 = 4\delta/T_s$, MAK is better than FP. However that advantage is appreciable only if $T_s \ll T_m$. A comparison between the systems is illustrated in Fig. 5. It is worth recalling that throughout this paper we consider MAK at the r points such that, for MAK, Fig. 5 applies only for δ and l corresponding to the r-point condition, i.e., when the shorter subcavity is on resonance while the longer one is on antiresonance.

VII. OPTIMIZATION OF AN OPTOMECHANICAL SETUP

Above, when discussing the advantages and disadvantages of various configurations containing a highly reflecting membrane, we felt free to manipulate all the parameters of each system. However, in practice, the experimenter will seek to obtain the highest figure of merit for their application with a given highly reflecting membrane. Let us fix the parasitic loss T_s and the minimum membrane transmission $T_{m,\rm min}$ while allowing the membrane transmission be widely tunable above this value by changing the operating wavelength. The other quantities, which are in the hands of the experimenter, are as follows: the separation δ between the membrane and the adjacent mirror, the overall length of the cavity l, and the coupling

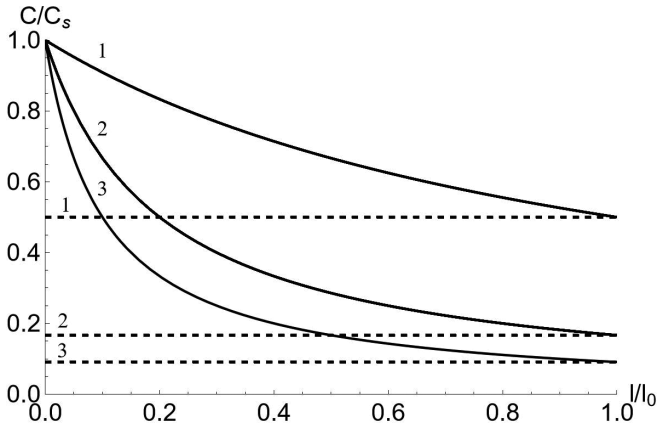

FIG. 5. The normalized cooperativity C_{FP}/C_s of FP (dashed lines) and C_{MAK}/C_s of MAK (solid lines), plotted as a function of the normalized length of the cavity l/l_0, where $l_0 = 4\delta/T_s$ and $C_s = 8(\omega_c x_{\mathrm{zpf}})^2/(c\gamma_m \delta T_s)$ is the cooperativity of FP in the limit where the loss is fully dominated by the parasitic scattering. Curves numbered 1, 2, and 3 are plotted for $T_m/T_s = 2$, 5, and 10, respectively. The situation of practical interest where $T_s \gg TT_m/4$ is addressed.

mirror transmission T. All schemes favor a small δ. Thus, it should be minimized. A membrane-mirror separation down to $1.6 \pm 0.8\,\mu$m was reported in [10]. Once the achievable δ has been chosen, we can discuss optimal choices for the remaining free parameters.

It was shown above that with respect to the cooperativity, the best configurations are MAK and FP, although with respect to the weighted cooperativity FP is always the best. For this reason, we address the optimization of MAK or FP with respect to the cooperativity and FP with respect to the weighted cooperativity.

Starting from the weighted cooperativity of FP, via Eqs. (51) and (52), we readily find that it is maximal when the external loss matches the internal loss, i.e., at $T_m = T_s$. If, however, $T_{m,\min} > T_s$, to maximize the weighted cooperativity, one should set $T_m = T_{m,\min}$.

When discussing the optimization with respect to the cooperativity we restrict ourselves to the realistic situation where $T_s \gg TT_m/4$ such that Eqs. (55) and (56) and Fig. 5 can be used. First, we see that to maximize the gain from the use of a highly reflecting membrane one should use MAK with a cavity shorter than $l_0 = 4\delta/T_s$. Second, following from (56), for a fixed cavity length, a further maximization of the cooperativity is possible through a reduction of the membrane transparency T_m. One can also readily check that the maximal gain of MAK over FP is T_m/T_s. Since T_s can be as small as 10^{-3}–10^{-4} [11–13], such a gain can still be appreciable.

VIII. CONCLUSIONS

We presented an analysis of the problem of the optimal position of a highly reflecting membrane in a one-sided cavity. In our analysis, we addressed the coupling constant and the figures of merit of an optomechanical device such as the cooperativity and efficiency-weighted cooperativity. These figures of merit are relevant in different situations; e.g., for optomechanical cooling the cooperativity matters, while it is the efficiency-weighted cooperativity that matters for optical sensing of the mechanical subsystem. We found that the optimal settings for these figures of merit are very different.

In contrast to previous theoretical considerations of an optical cavity with a membrane inside [1,2,10], here, we incorporated the parasitic scattering of the membrane while neglecting the parasitic scattering from the coupling mirror, which we assume is much weaker than that from the membrane. We demonstrated that, in the case of a highly reflecting membrane, even a small amount of parasitic scattering from the membrane may have an essential impact on the cooperativity of the system.

The regimes with the membrane close to the coupling mirror (MATE), close to the backstop mirror (MAK), and close to the cavity center (MIM) were compared. The comparison was done for the points of the spectrum where g_0 is less affected by the effect of the avoided crossing of the resonance modes of the two subcavities, which we called r points. A remarkable feature of MAK and MATE at the r points is that the shorter subcavity is on resonance, while the longer one is on antiresonance, such that MATE can be viewed as a short cavity with a synthetic backstop mirror and MAK can be viewed as one with a synthetic coupling mirror. In this context, we compared the optomechanical parameters of MATE and MAK with those of a one-sided FP cavity with a membrane used as the coupling mirror, with its length δ being equal to the separation between the membrane and the adjacent mirror in MAK or MATE.

We found that, with respect to the coupling constant and the efficiency-weighted cooperativity, FP is the best of all the systems addressed. However, in terms of the cooperativity, the situation is different. Among MIM, MATE, and MAK, the latter is always the best, although, in some regimes, the performance of MATE can be very close to that of MAK. Comparing MAK with FP, we found that each of them can be superior, depending on the parameters of the system. First, in the limit of very weak parasitic scattering, the regime where $T_s \ll TT_m/4$, MAK is superior over FP by a factor of about $\frac{4(T_m+T_s)}{T_m T}$. Thus, in this regime, MAK would provide an extraordinary performance. However, even a very small amount of parasitic scattering from the membrane can essentially suppress the performance of MAK. This happens when T_s is comparable to or larger than $TT_m/4$. The situation of practical interest is $T_s \gg TT_m/4$. In this regime, FP can compete with MAK; specifically, if the cavity length l used in MAK exceeds $l_0 = 4\delta/T_s$, the cooperativity of FP is larger than that of MAK. For shorter cavities, the cooperativity of MAK is larger than that of FP. For membranes with parasitic scattering much weaker than the transmission, i.e., for $T_s/T_m \ll 1$ and $l \ll 4\delta/T_s$, this advantage is appreciable, being about T_m/T_s.

All in all, in terms of cooperativity, for the optomechanical setups using a highly reflecting membrane placed inside an optical cavity, the MAK configuration was shown to be advantageous compared to other configurations. However, in this respect, in a certain regime, the performance of MATE can be very close to that of MAK. In addition, in terms of cooperativity, MAK can also be advantageous compared to FP with the membrane as the coupling mirror with the same membrane-mirror separation as MAK. In the regime of extremely weak parasitic scattering of the membrane, MAK

can provide very high cooperativity. Outside of this regime, which currently is a realistic experimental situation, MAK can be tuned to yield a cooperativity larger than that of FP. This advantage can be essential only for a membrane exhibiting parasitic scattering appreciably weaker than its transmission. If one cares about the efficiency-weighted cooperativity, the use of a highly reflecting membrane is optimal when it serves as the coupling mirror of a FP cavity.

Data underlying the results presented in this paper are not publicly available at this time but may be obtained from the authors upon reasonable request.

ACKNOWLEDGMENTS

G.E. acknowledges support from the European Union's Horizon 2020 research and innovation program under Marie Sklodowska-Curie Grant Agreement No. 847523. E.S.P. was supported by VILLUM FONDEN under Villum Investigator Grant No. 25880. The authors acknowledge insightful discussions with A. Simonsen and Z. Wang.

The authors declare no conflicts of interest.

APPENDIX A: FREQUENCY GAP AT THE CROSSING POINTS

In this Appendix, we evaluate the frequency gap which appears at a crossing point of the spectrum of the subcavities of the systems (see Fig. 1) once weak coupling between these is allowed. A form of Eq. (8) that is proper for further analysis reads

$$\cos[k(l-x)+\varphi_r/2]\cos(kx+\varphi_r/2)=\frac{t_m^2}{4}\cos(2kx-kl). \tag{A1}$$

Let x_0 and k_0 be the membrane position and the resonant wave number corresponding to a crossing point, respectively. At these points, both subcavities are on resonance, such that both cosines in (A1) should be equal to zero:

$$\cos[k_0(l-x_0)+\varphi_r/2]=0, \quad \cos(k_0x_0+\varphi_r/2)=0. \tag{A2}$$

Next, looking for the solution to Eq. (A1) in the form $x=x_0$ and $k=k_0+\delta k$, we find, in the limit of small t_m, that

$$\delta k^2 \propto \frac{t_m^2}{x_0(l-x_0)}, \tag{A3}$$

implying (9).

APPENDIX B: PROPERTIES OF THE SYSTEM AT THE R POINTS

This Appendix addresses some properties of the system at the r points. Let us show that, with the variation of t_m, the $\omega(x)$ curves "locally rotate" about the r points. To be specific let us consider the r points formed by the intersection of the $\omega(x)$ curves for the $\omega_{\rm L}$ mode calculated at $t_m=0$ and $t_m\neq 0$. Since we are on the resonance curve for the x-long part of the cavity, the phase shift on reflection from the membrane equals φ_r. Thus, taking into account that the round-trip phase variation along any loop should be equal to 2π times an integer, we can write

$$e^{i(2kx+\pi+\varphi_r)}=1. \tag{B1}$$

For the $(l-x)$-long part, we can write the following round-trip phase condition:

$$e^{i[2k(l-x)+\pi+\mu]}=1, \tag{B2}$$

where μ is the phase shift at the reflection from the x-long part. Since the $(l-x)$-long part is not on resonance, $\mu\neq\varphi_r$. These two equations specify the positions of the corresponding r points. On the other hand, we can readily check that the phase shift on reflection from a one-sided cavity on resonance is independent of the transmission of the input mirror (see Appendix C). In our case,

$$\mu=\varphi_r-\pi. \tag{B3}$$

Thus, μ is independent of the membrane transmission, implying the independence of the positions of the r points.

For the $\omega_{\rm L}$ modes, Eqs. (B1), (B2), and (B3) can be rewritten as follows:

$$e^{-2ik(l-x)-i\varphi_r}=1, \quad e^{-2ikx-i\varphi_r}=-1. \tag{B4}$$

Similar expressions can be readily shown for the $\omega_{\rm R}$ modes:

$$e^{-2ik(l-x)-i\varphi_r}=-1, \quad e^{-2ikx-i\varphi_r}=1. \tag{B5}$$

Equations (B4) and (B5) imply that, at the r points, one of the subcavities is on resonance, while the other is on antiresonance.

For the r points, we also evaluate the ratio of the field intensity in one part of the cavity to that in the other part. We will first consider this for an $\omega_{\rm L}$ mode. Based on Eq. (C2), we consider the following complex amplitude balance equation at the membrane (see Fig. 1 for the definition of the amplitudes):

$$B=t_me^{i\varphi_s}A+r_me^{i\varphi_r}G\,. \tag{B6}$$

Since, at the r points considered, the x-long part is on resonance, using (B3), we can write

$$B=e^{i(\varphi_r-\pi)}G. \tag{B7}$$

Combining equations (B6) and (B7), in the limit $t_m\ll 1$, we find

$$\frac{|B|^2}{|A|^2}=\frac{T_m}{4}, \tag{B8}$$

where $T_m=t_m^2$ is the power (intensity) transmission of the membrane and $|A|^2$ and $|B|^2$ are the intensities in the x-long and $l-x$-long parts of the cavity, respectively.

For the r points of the $\omega_{\rm R}$ mode, similar calculations yield

$$\frac{|B|^2}{|A|^2}=\frac{4}{T_m}. \tag{B9}$$

Next, we find the mirror-membrane separation, labeled $x_{\rm int}$, at which, for the r points, the energy of a mode stored in one subcavity is equal to that stored in the other. Evidently, $x_{\rm int}$ is given by the solution to the equation

$$x|A|^2=(l-x)|B|^2, \tag{B10}$$

such that, for a highly reflecting membrane, using (B8) and (B9), we find

$$x_{\rm int} = l\frac{T_m}{4}. \tag{B11}$$

For the $\omega_{\rm L}$ modes, (B11) gives the membrane separation from the coupling mirror, while for the $\omega_{\rm R}$ modes, it is the separation from the backstop mirror.

APPENDIX C: REFLECTION FROM RESONANCE CAVITY

Consider only the membrane and the backstop mirror as in Fig. 1 when the $l-x$ long part of the cavity is on resonance, i.e., according to (13),

$$e^{-2ik_0(l-x)-i\varphi_r} = -1. \tag{C1}$$

According to (2), (3), and (4) the complex amplitudes are linked by the following relations:

$$\begin{aligned} B &= -Fe^{-2ik(l-x)},\\ B &= t_m e^{i\varphi_t}A + r_m e^{i\varphi_r}G,\\ F &= r_m e^{i\varphi_r}A + t_m e^{i\varphi_t}G. \end{aligned} \tag{C2}$$

Eliminating B and C between set (C2) and taking into account (C1), we find

$$\frac{F}{A} = -e^{i\varphi_r}, \tag{C3}$$

implying that the phase of the signal reflected from a cavity on resonance is independent of the modulus of the reflection coefficient of the coupling mirror.

APPENDIX D: COUPLING CONSTANT AND DECAY RATE

Equations (1), (2), (3), and (4) lead to the following relations between the complex amplitudes (see Fig. 1):

$$\begin{aligned} A &= -rFe^{2ikx},\\ B &= -Ge^{-2ik(l-x)},\\ B &= t_m e^{i\varphi_t}A + r_m e^{i\varphi_r}G,\\ F &= r_m e^{i\varphi_r}A + t_m e^{i\varphi_t}G, \end{aligned} \tag{D1}$$

which imply the following equation for the resonance wave vector (in general, complex):

$$(r_m + e^{-2ik(l-x)-i\varphi_r})(r_m + r^{-1}e^{-2ikx-i\varphi_r}) + t_m^2 = 0. \tag{D2}$$

Since the dissipation is assumed to be weak, to find g_0, we neglect it by setting $r=1$ and $t_m^2 = 1-r_m^2$ to find

$$(r_m + e^{-2ik(l-x)-i\varphi_r})(r_m + e^{-2ikx-i\varphi_r}) + 1 - r_m^2 = 0, \tag{D3}$$

which is equivalent to (8). The derivative dk/dx calculated on the resonance using (D3) reads

$$\frac{dk}{dx} = \frac{\omega_c}{c}\frac{e^{-2ik(l-x)-i\varphi_r}(r_m + e^{-2ikx-i\varphi_r}) - e^{-2ikx-i\varphi_r}(r_m + e^{-2ik(l-x)-i\varphi_r})}{(l-x)e^{-2ik(l-x)-i\varphi_r}(r_m + e^{-2ikx-i\varphi_r}) + xe^{-2ikx-i\varphi_r}(r_m + e^{-2ik(l-x)-i\varphi_r})}. \tag{D4}$$

For the r points of the $\omega_{\rm R}$ mode where the $l-x$ long subcavity is on resonance while the other subcavity is on antiresonance, i.e., $e^{-2ik_0(l-x)-i\varphi_r} = -1$ and $e^{-2ik_0x-i\varphi_r} = 1$, we find

$$\frac{dk}{dx} = \frac{\omega_c}{c}\frac{r_m}{(l-x)r_m + lt_m^2/4}, \tag{D5}$$

which, in the approximation $t_m^2 \ll 1$, readily yields (22).

For the r points of the $\omega_{\rm L}$ modes where $e^{-2ik_0(l-x)-i\varphi_r} = 1$ and $e^{-2ik_0x-i\varphi_r} = -1$, along the same lines, we obtain (21) as well.

To evaluate the cavity decay rate, we rewrite (D2) as follows:

$$(r_m + e^{-2ik(l-x)-i\varphi_r})(r_m + r^{-1}e^{-2ikx-i\varphi_r}) + 1 - r_m^2 = T_s. \tag{D6}$$

We expand (D6) about k_0, which is the solution to (D3); keeping the lowest term in $t^2 \ll 1$ and $\delta k = k - k_0$, we find

$$\delta k = -\frac{i}{2}\frac{T_s + (1-r^{-1})e^{-2ikx-i\varphi_r}(r_m + e^{-2ik(l-x)-i\varphi_r})}{(l-x)e^{-2ik(l-x)-i\varphi_r}(r_m + e^{-2ikx-i\varphi_r}) + xe^{-2ikx-i\varphi_r}(r_m + e^{-2ik(l-x)-i\varphi_r})}. \tag{D7}$$

Now, using the above resonance-antiresonance conditions for the subcavities, for the $\omega_{\rm R}$ mode, we arrive at the following cavity decay rate:

$$\kappa = -2c{\rm Im}[\delta k] = \frac{c}{2}\frac{T_S + (r^{-1}-1)(1-r_m)}{(l-x)r_m + lt_m^2/4}, \tag{D8}$$

which, under the conditions $1-r_m \approx T_m/2 \ll 1$ and $1-r \approx T/2 \ll 1$, readily brings us to (33) and (34). Along the same lines, we obtain (36) and (37).

[1] A. M. Jayich, J. C. Sankey, B. M. Zwickl, C. Yang, J. D. Thompson, S. M. Girvin, A. A. Clerk, F. Marquardt, and J. G. E. Harris, New J. Phys. **10**, 095008 (2008).
[2] H. Miao, S. Danilishin, T. Corbitt, and Y. Chen, Phys. Rev. Lett. **103**, 100402 (2009).
[3] Y. Yanay, J. C. Sankey, and A. A. Clerk, Phys. Rev. A **93**, 063809 (2016).
[4] J. D. Thompson, B. M. Zwickl, A. M. Jayich, F. Marquardt, S. M. Girvin, and J. G. E. Harris, Nature (London) **452**, 72 (2008).
[5] D. J. Wilson, C. A. Regal, S. B. Papp, and H. J. Kimble, Phys. Rev. Lett. **103**, 207204 (2009).
[6] T. P. Purdy, P.-L. Yu, R. W. Peterson, N. S. Kampel, and C. A. Regal, Phys. Rev. X **3**, 031012 (2013).
[7] D. Mason, J. Chen, M. Rossi, Y. Tsaturyan, and A. Schliesser, Nat. Phys. **15**, 745 (2019).
[8] N. S. Kampel, R. W. Peterson, R. Fischer, P.-L. Yu, K. Cicak, R. W. Simmonds, K. W. Lehnert, and C. A. Regal, Phys. Rev. X **7**, 021008 (2017).
[9] A. P. Higginbotham, P. S. Burns, M. D. Urmey, R. W. Peterson, N. S. Kampel, B. M. Brubaker, G. Smith, K. W. Lehnert, and C. A. Regal, Nat. Phys. **14**, 1038 (2018).
[10] V. Dumont, S. Bernard, C. Reinhardt, A. Kato, M. Ruf, and J. C. Sankey, Opt. Express **27**, 25731 (2019).
[11] X. Chen, C. Chardin, K. Makles, C. Caër, S. Chua, R. Braive, I. Robert-Philip, T. Briant, P.-F. Cohadon, A. Heidmann, T. Jacqmin, and S. Deléglise, Light: Sci. Appl. **6**, e16190 (2017).
[12] G. Enzian, Z. Wang, A. Simonsen, J. Mathiassen, T. Vibel, Y. Tsaturyan, A. Tagantsev, A. Schliesser, and E. S. Polzik, Opt. Express **31**, 13040 (2023).
[13] F. Zhou, Y. Bao, J. J. Gorman, and J. R. Lawall, Laser Photon. Rev. **17**, 2300008 (2023).
[14] D. J. Wilson, V. Sudhir, N. Piro, R. Schilling, A. Ghadimi, and T. J. Kippenberg, Nature (London) **524**, 325 (2015).
[15] A. K. Tagantsev, I. V. Sokolov, and E. S. Polzik, Phys. Rev. A **97**, 063820 (2018).

Correction: The values given for t_m in the caption of Figure 3 were incorrect and have been fixed.